Electron affinities of small-molecule organic semiconductors: Comparison among cyclic voltammetry, conventional inverse photoelectron spectroscopy, and low-energy inverse photoelectron spectroscopy

Mihiro Kubo[a], Hiroyuki Yoshida[b, c, *]

[a]Graduate School of Science and Engineering, Chiba University, 1-33 Yayoi-cho, Inage-ku, Chiba 263-8522, Japan

[b]Graduate School of Engineering, Chiba University, 1-33 Yayoi-cho, Inage-ku, Chiba 263-8522, Japan

[c]Molecular Chirality Research Center, Chiba University, 1-33 Yayoi-cho, Inage-ku, Chiba 263-8522, Japan

*Corresponding author

E-mail address: hyoshida@chiba-u.jp (H. Yoshida)

Abstract

The electron affinity (A) of an organic semiconductor is an energy parameter representing the electron transport level. The precise value of A in a solid is indispensable for examining and designing organic semiconductor devices. In principle, A in a solid can be determined by inverse photoelectron spectroscopy (IPES). However, because IPES is normally available only for specialists of IPES, A is often estimated from the reduction potential E_{red} measured in solution using a more easily available method, cyclic voltammetry (CV). Thus, the conversion relation from E_{red} into A is practically important in the research of organic semiconductors. On the other hand, previous IPES data may have errors of about 0.3–0.5 eV owing to sample damage and low energy resolution. In 2012, one of the authors developed low-energy inverse photoelectron spectroscopy (LEIPS), which enables the determination of A with the precision of 0.1 eV. In this work, we establish the correlation between CV data E_{red} and solid-state A based on LEIPS data and suggest the relation $A = (1.24 \pm 0.07) \times e\ E_{red} + (5.06 \pm 0.15)$ eV. We also discuss the reliability of the A values determined by the previous IPES and the present LEIPS in terms of the LUMO spectral onset and the vacuum level.

Keywords

low-energy inverse photoelectron spectroscopy; cyclic voltammetry; electron affinity; reduction potential; LUMO level; organic semiconductor

1. Introduction

Electronic devices designed with organic semiconductors are regarded as next-generation electronic devices that are inexpensive, flexible, lightweight, and eco-friendly because a high-temperature process is not required for fabrication. Organic light-emitting diodes have already been commercially available for more than two decades, and other devices such as organic solar cells and organic transistors are being intensively studied. Information on the energy level is essential for designing these devices and choosing the most appropriate organic semiconductor. In particular, the energy levels of the highest occupied molecular orbital (HOMO) and the lowest unoccupied molecular orbital (LUMO) are important for hole and electron conductions, respectively. The energy levels of HOMO and LUMO are represented by the ionization energy I and the electron affinity A, respectively, which are the energies with reference to the vacuum level. Therefore, a quick and reliable method for determining I and A are required.

As thin films of organic semiconductors are used in actual devices, we need to measure the energy levels of the films, i.e., measurements of energy levels in a solid are necessary. For measuring I in a solid, ultraviolet photoelectron spectroscopy (UPS) and photoelectron yield spectroscopy (PYS) are routinely used. Conversely, A can be measured by inverse photoelectron spectroscopy (IPES), which can be regarded as the inverse process of UPS. However, a theoretical study revealed that the cross section for IPES is 10^{-3} to 10^{-5} times smaller than that for UPS [1]. Therefore, we need to irradiate a sample with a high-intensity electron beam and use a specially designed high-sensitivity photon detector to observe weak photon signals [2-4]. This, however, leads to damage of organic semiconductor molecules caused by electron bombardment [5] and a low energy resolution of about 0.5 eV in practical measurements. The A values determined by IPES are often assumed to have an uncertainty of 0.3–0.5 eV [6, 7].

In 2012, Yoshida developed low-energy inverse photoelectron spectroscopy (LEIPS) [8, 9]. In LEIPS, the kinetic energy of electrons is decreased to below 5 eV, which is the damage threshold of most organic materials. With the decrease in electron energy, the photon energy also decreases to near the ultraviolet range, which enables us to use a high-resolution bandpass filter and a high-efficiency photomultiplier tube for photon detection. As a result, A of organic samples can be determined with a precision of 0.1 eV similarly to I determined by UPS. Taking advantage of the high accuracy of LEIPS, we have examined the interface energy level alignment of LUMO levels [10], the electrostatic energy and electronic polarization energy in organic thin films [11-15], and the conduction band structure of organic-inorganic hybrid perovskite [16].

However, UPS, LEIPS, and IPES are not always accessible to ordinary research groups because the measurements have to be conducted in ultrahigh vacuum using an expensive apparatus and a specialist is often required for operation. As an alternative method that is easy to use and generally available, cyclic voltammetry (CV) is widely used. In CV, the oxidation (reduction) potential E_{ox} (E_{red}) of a

material in solution is measured on the basis of electrochemical reactions. Often, the first oxidation potential of 4.8 eV of the ferrocenium/ferrocene (Fc^+/Fc) system is used as a reference. Thus, $I(A)$ is estimated as follows:

$$I(A) = e\,E_{ox}\ (e\,E_{red}) + 4.8\ \text{eV}, \qquad (1)$$

where e is the elemental charge. For a more precise conversion, considering the oxidation (reduction) reaction near the electrodes, the relationship between I (A) and E_{ox} (E_{red}) may be expressed by the linear relations

$$I = \alpha^+ \times e\,E_{ox} + \beta^+, \qquad (2)$$

$$A = \alpha^- \times e\,E_{red} + \beta^-. \qquad (3)$$

On the basis of the comparison of I measured by UPS with that measured by CV, the empirical parameters $\alpha^+ = (1.4 \pm 0.1)$, $\beta^+ = (4.6 \pm 0.08)$ [17], $\alpha^+ = (1.15 \pm 0.09)$, $\beta^+ = (4.79 \pm 0.07)$ [7], and $\alpha^+ = (1.7 \pm 0.2)$, $\beta^+ = (4.6 \pm 0.1)$ [18] have been proposed. From A measured by conventional IPES, $\alpha^- = (1.19 \pm 0.08)$, $\beta^- = (4.78 \pm 0.17)$ [6], and $\alpha^- = (1.18 \pm 0.05)$, $\beta^- = (4.83 \pm 0.10)$ [7] have been evaluated. However, as mentioned above, the precision of A values determined by conventional IPES has been questioned and the parameters α and β are needed to be reexamined.

In this study, we reevaluate the parameters α^- and β^- in Eq. 3 using the A values determined by LEIPS. The correlation coefficients depend on the choice of the materials [7]. We restrict our work to small-molecule organic semiconductors. Materials for the state-of-the-art organic photovoltaic cells such as low-bandgap polymers and non-fullerene acceptors will be discussed elsewhere. The differences in the parameters α^- and β^- between the literature and this study should arise from the difference between the data determined by LEIPS and conventional IPES. We further discuss LEIPS and conventional IPES measurements in terms of the determination of the LUMO onset and the vacuum level (workfunction).

2. Results and Discussion

Table S1 and Figure S1 show the molecules examined in this work. The energy parameters E_{red} [6, 19-25] and A [8-10, 12, 15, 25-28] are taken from the literature. For E_{red}, we selected 25 data measured only with reference to the ferrocenium/ferrocene (Fc^+/Fc) potential to avoid systematic error. Ten of the 25 data are the same as those employed in a previous study [7]. We found no discernible difference by adding the new data (Fig. S1), confirming that the reported E_{red} values are precise and reproducible.

Figure 1 show the correlation between A measured by LEIPS and E_{red} measured by CV. We found a good linear correlation between A and E_{red}, which is expressed as

$$A = (1.24 \pm 0.07) \times e\,E_{red} + (5.06 \pm 0.15)\ \text{eV}, \qquad (4)$$

with $R^2 = 0.93$. The slope α^- in Eq. 4 is about 0.1 eV larger than those in previous studies by Sworakowski et al. [7] and Djurovich et al. [6]. The onset β^- should be close to the first oxidation

potential of 4.8 eV of the Fc^+/Fc system. The β^- agrees within the uncertainty. Practically, the A values calculated from the present and previous works are only different by less than 0.2 eV in the entire region, and 0.1 eV in the energy range of E_{red} <-2.0 eV. This means that the previous discussion based on the A values having the larger uncertainties obtained by the conventional IPES [6,7] holds. Note the parameters α and β are similar between Refs. [6] and [7] because mostly the same IPES data were used in these studies.

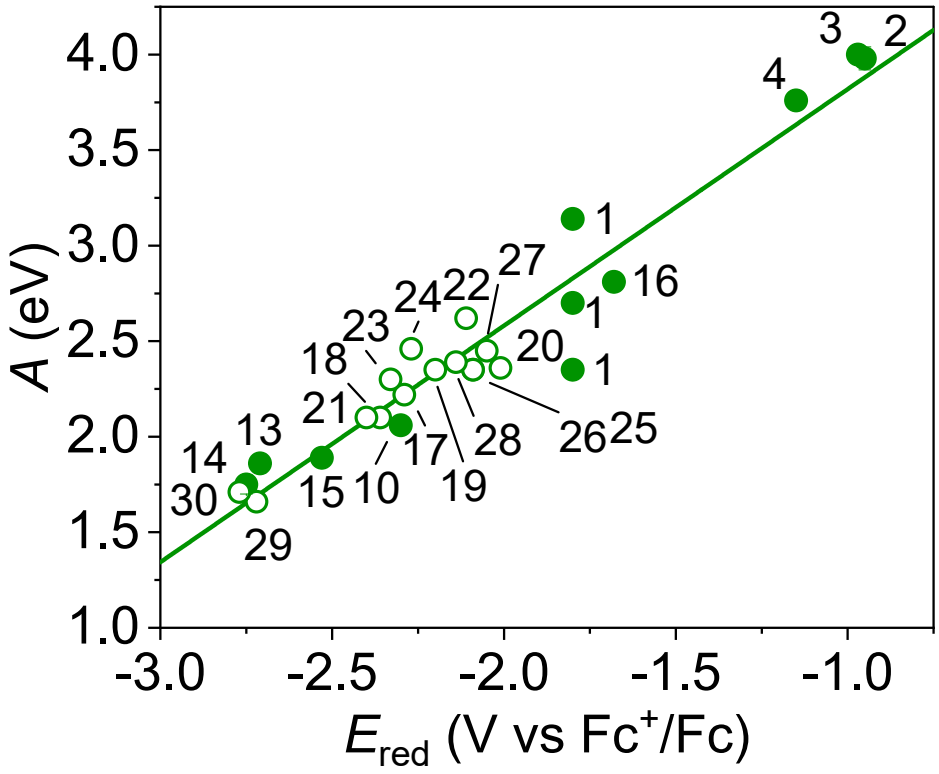

Fig. 1 Correlation between A measured by LEIPS and E_{red} measured by CV. The data are shown in Table S1 for 23 compounds identified by the entry numbers. The data of the materials whose molecular structures are undisclosed are shown by open circles. The solid line is the linear correlation determined by the least squares method.

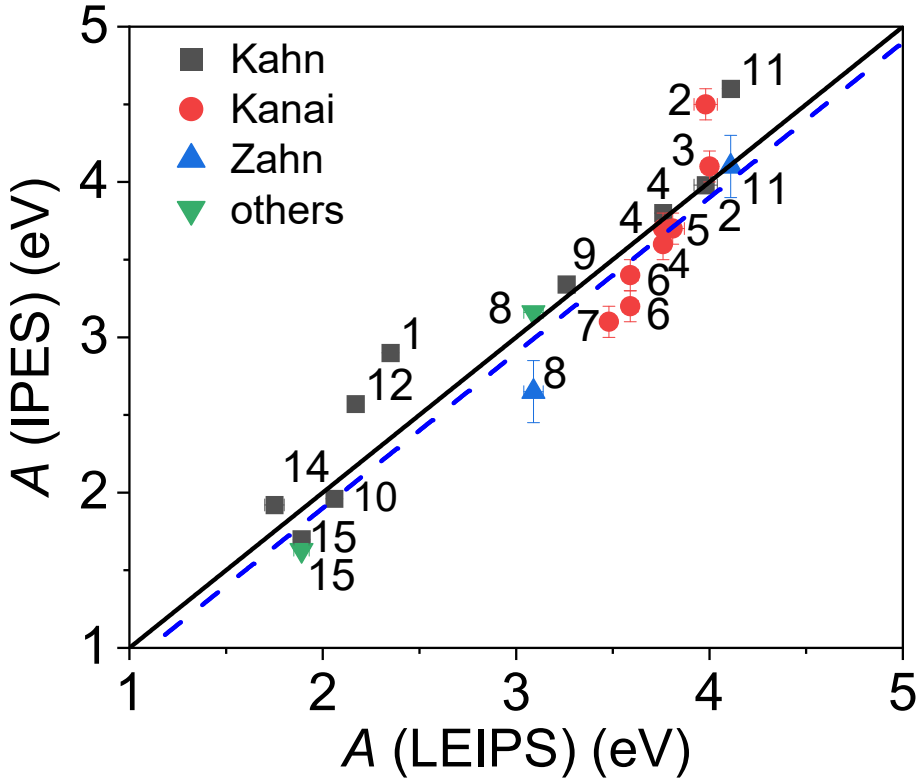

Fig. 2 Correlations between *A* measured by IPES and that measured by LEIPS. The data are shown in Table S1 for the 14 compounds whose molecular structures are shown in Fig. S1. The solid line (black) is depicting a linear relationship passes the origin with the slope of unity. In the case of the blue dashed line, its intercept is shifted by 0.1 eV to account for the workfunction difference between the LEET method and SECO onset by UPS (see text).

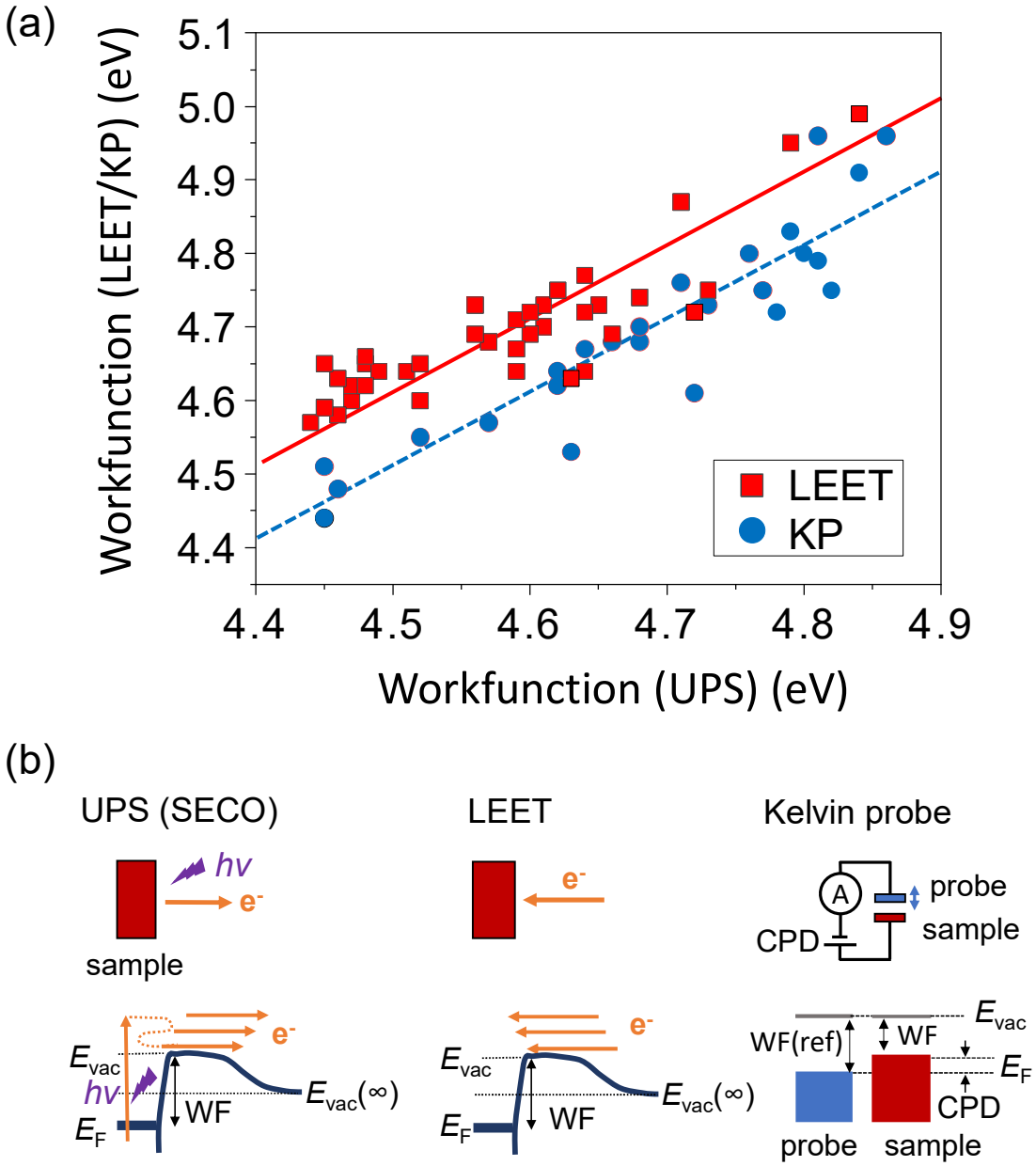

Fig. 3 (a) Correlations between the experimental workfunctions of polycrystalline Ag determined by LEET method (squares) and KP method (circles), and the workfunction by SECO onset by UPS. The solid line (red) is the linear correlation between the workfunction determined by LEET method and that by SECO onset by UPS. The dashed line (blue) is the linear correlation between the workfunction determined by the KP method and that determined by SECO onset by UPS. (b) The experimental methods for the workfunction illustrated together with their energy diagrams.

The difference between the A values from the previous studies [6, 7] and those from this study originates from the measurement method, that is, IPES or LEIPS. Figure 2 shows the correlation

between LEIPS data and conventional IPES data. Because the values may depend on the experimental apparatus and the method of data analysis, the conventional IPES data are indicated separately by research groups. *A* is the onset (threshold) of the LEIPS or IPES spectrum with respect to the vacuum level. In practical experiments, the onset of the LUMO-derived peak and the vacuum level (workfunction) are measured separately with reference to the Fermi level. Therefore, we discuss below the difference in the determination of the onset of LUMO level and the vacuum level separately.

The vacuum level can be determined by three methods: (1) the onset of secondary electron cutoff (SECO) by UPS, (2) the low-energy electron transmission (LEET) method, and (3) the Kelvin probe (KP) method, as illustrated in Fig. 3. The groups of Kahn in Princeton University, Kanai in Nagoya University/Okayama University/Tokyo University of Science, and Zahn in Chemnitz University of Technology used SECO onset by UPS measurement of the same sample. In this method, the threshold energy of the outgoing secondary electrons travelling beyond the energy barrier at the sample surface [29] is measured using an electron energy analyzer [Fig. 3(b)]. As the energy resolution is much better than 100 meV, which is sufficiently higher than the uncertainty of the LUMO onset, the SECO onset is usually used to determine the vacuum level. On the other hand, the vacuum level is determined by the LEET method by Sato's group in Kyoto University and Yoshida's group in Kyoto University/Chiba University. In the LEET method, the sample current is measured by introducing an electron beam as a function of electron kinetic energy [Fig. 3(b)]. The vacuum level is determined as the threshold energy of incoming electrons. However, the energy of the electron beam is increased by about 0.25 eV by the thermal spread $2kT$ of the cathode (T = 1100–1300 K). Thus, the vacuum level is determined not by the onset but by the inflection point of the LEET spectrum.

In these two methods, the vacuum level is determined as the threshold energy of outgoing or incoming electrons from or toward the sample surface, respectively. Therefore, measurements of SECO onset by UPS and the LEET method give the same value in principle. We examined the correlation between the workfunctions determined by the LEET method (Φ_{LEET}) and SECO onset by UPS (Φ_{UPS}) for polycrystalline Ag, as shown in Fig. 3. We found a good linear relationship, as shown by the fit to a line with a slope of unity:

$$\Phi_{LEET} = \Phi_{UPS} + (0.11 \pm 0.0085) \qquad (5)$$

with $R^2 = 0.74$. The onset of 0.11 eV is the systematic difference mainly due to the energy resolution and the determination of the threshold values.

The vacuum level (workfunction) can also be determined by the KP method based on the contact potential difference (CPD) between the surfaces of the sample and the reference electrode [Fig. 3(b)]. Because no net electron current is induced in KP measurements, the measurement is not affected by the sample charging. Taking advantage of this feature of the KP method, the thickness dependence of the workfunction was determined for a C_{60} layer up to a thickness of 500 nm [30], which usually cannot be examined by SECO onset by UPS or the LEET method. We examined the same

polycrystalline Ag surface (Fig. 3) and obtained the relationship between Φ_{KP} and Φ_{UPS} as

$$\Phi_{KP} = \Phi_{UPS} + (0.01 \pm 0.011) \quad (6)$$

with $R^2 = 0.83$. Note that the KP data shown in Fig. 3 were obtained in vacuum. When workfunction measurements using the KP method were conducted in an inert gas, we were not able to obtain a reliable result. This means that the workfunction measured by the KP method is sensitively affected by the surfaces of the sample and the reference electrode.

In contrast to metal surfaces, organic semiconductor films may be affected by sample charging, which can further cause the difference in the workfunctions measured by SECO onset by UPS and the LEET method. The sample current is typically 1 nA in UPS, whereas the current is 100–1000 times larger (0.1–1 μA) in the LEET method and LEIPS. As a result, sample charging may more severely affect workfunction measurements in the LEET method. Figure 4 shows the workfunctions determined by SECO onset by UPS and the LEET method for perylene-3,4,9,10-tetracarboxylic dianhydride (PTCDA) film evaporated on Au(111). The workfunction determined by the LEET method is larger by 0.1 eV than that by SECO onset by UPS when PTCDA film thickness is less than 3 nm. The difference is similar to that observed for polycrystalline Ag discussed above, and is understandable from the determination of the onset energies. However, in the film with more than 4 nm thickness, the workfunction determined by the LEET method becomes larger than that by SECO onset by UPS by about 0.2 eV. The difference can be explained by the slight charging of the sample surface; the PTCDA film becomes negatively charged upon the introduction of an electron beam and the threshold energy of the incoming electrons becomes large, leading to a larger workfunction. For the precise measurement of A, the simultaneous measurement of the LUMO onset by IPES (LEIPS) and the workfunction by the LEET method is more advantageous than the separate measurement of the LUMO onset and the workfunction by SECO onset. The slight sample charging increases the electrostatic potential around the sample molecule to be measured. This electrostatic potential is expected to shift the LUMO onset and the workfunction simultaneously without changing A. The workfunction determined separately by SECO onset by UPS cannot take this effect of the charging into account.

Because the workfunction determined by SECO onset by UPS is about 0.1 eV smaller than that by the LEET method, A determined by the combination of conventional IPES and SECO onset is smaller than that by LEIPS and the LEET method if the onset of LUMO levels is unchanged. The blue dashed line in Fig. 2 shows the relationship between A determined by IPES and that determined by LEIPS, taking the 0.1 eV difference in the workfunction into consideration. Several data points are on or below the straight line, which can be explained by the difference in the workfunction. However, the other data points above the line (A obtained by IPES is higher than that obtained by LEIPS) cannot be explained by the workfunction difference. We need to consider other factors that affect measured A, such as the energy resolution and the radiation-induced damage. The energy resolution of conventional IPES is practically 0.5 eV, which is two times lower than that of LEIPS (0.25 eV). This lower energy

resolution may increase *A*. We roughly estimate the effect of peak broadening on *A*. Suppose that intrinsic peak width is σ_1 = 1 eV. The energy resolution (instrumental broadening) of LEIPS σ_2= 0.25 eV yields the observed peak width of $(\sigma_1^2+ \sigma_2^2)^{1/2}$=1.03 eV, whereas that of conventional IPES σ_2= 0.5 eV gives $(\sigma_1^2+ \sigma_2^2)^{1/2}$=1.12 eV. The lower energy resolution of conventional IPES almost compensates for the difference in workfunction of about 0.1 eV, and as a result, the *A* values measured by IPES and LEIPS become almost the same.

There can be several origins that can cause the large deviation from the straight line in Fig. 2. In the films, *A* depend on the crystallinity [10], molecular orientation [13-15], and sample shape [31]. For example, *A* of $PC_{61}BM$ is larger in amorphous film (as-prepared) than in crystalline film (annealed) by 0.1 eV owing to the electronic polarization energy [10]. *A* of the molecules with a large permanent quadrupole may depend on the molecular orientation in a well-ordered film by up to 1 eV owing to the electrostatic potential generated by the molecular quadrupole moment [13-15]. The discrepancy in the pentacene and 6T data in Table S1 can be understood from the molecular orientation. In conventional IPES, the radiation-induced damage may not be neglected and may broaden the observed line shape. The radiation damage also affects the workfunction leading to the increase or decrease of *A*. The differences in the fullerenes (C60, bis-PCBM, ICBA) in Table S1 are likely caused by the radiation damage because the fullerenes have small quadrupole moments and are often randomly oriented in the film. The sensitivity to the electron bombardment depends on the materials and may differ by a few orders of magnitude [32]. The fairly good correlation between the LEIPS and conventional IPES data in Figure 2 suggests that the conventional IPES provides reliable *A* value if a durable molecule is carefully examined with avoiding the radiation-induced damage.

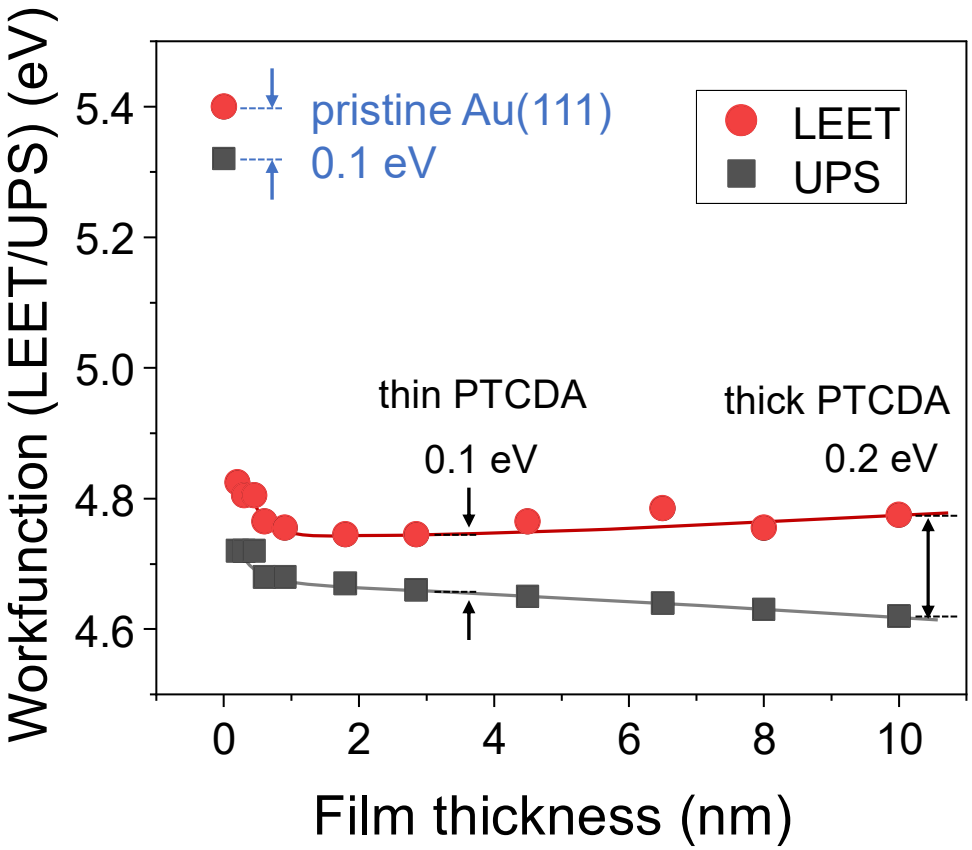

Fig. 4 Workfunction of PTCDA on Au(111) determined by LEET method and SECO onset by UPS as a function of film thickness. The solid lines are guides for the eyes.

3. Conclusion

The aim of this work is to develop a conversion method from the reduction potential E_{red} obtained from the electrochemical reaction in CV to the solid-state electron affinity A precisely determined by LEIPS. For this purpose, we analyzed the A values measured by three methods, namely, CV, conventional IPES, and LEIPS. Whereas conventional IPES has an uncertainty of 0.3–0.5 eV, LEIPS can measure A with a high precision of 0.1 eV.

The relationship between CV and conventional IPES has been examined in previous studies [6, 7]. In this study, we compared A measured by LEIPS with E_{red} measured by CV to obtain Eq. 4 with α^-=(1.24 ± 0.07), β^-=(5.06 ± 0.15) eV. Within the uncertainty, the obtained conversion relation is similar to those of the previous studies based on the conventional IPES data.

Because α^- and β^- were found to be different from those determined by conventional IPES reported in the literature (Eq. 3), we discussed the difference between A measured by conventional IPES and that by LEIPS (Fig. 2). The values are in fairly good agreement but may sometimes be inconsistent.

As *A* is determined as the energy difference between the vacuum level (workfunction) and the onset of the LUMO level, we separately investigated the workfunction and the LUMO onset to understand the origin of this discrepancy. The workfunction determined by the LEET method is about 0.1 eV larger than that by SECO onset by UPS. On the other hand, the onset energy of the LUMO level measured by conventional IPES differs from that by LEIPS because of the energy resolution and the sample damage. The effect of the energy resolution (instrumental broadening) is estimated to be less than 0.1 eV. Several *A* values measured by conventional IPES are largely deviate from those measured by LEIPS, which can be understood by the film crystallinity, the molecular orientation, and the radiation-induced damage.

Experimental Methods

UPS spectra were measured with He I light (photon energy hν = 21.22 eV). Photoelectron energy was analyzed using a PHOIBOS-100 analyzer (SPECS) or EA125 (Omicron).

Details of the LEIPS apparatus are described elsewhere [33]. The sample was perpendicularly irradiated with electrons having less than 5 eV kinetic energy and the emitted light was analyzed using a bandpass filter and a photomultiplier tube. To determine the Fermi level of Ag, we used the filter with a photon energy of 4.785 eV. For the electron affinities of organic samples, we used at least three different photon energies for higher precision. The LEET measurements were conducted with the electron kinetic energy below 2 eV. The workfunction was calculated as the energy of the inflation point (see main text) with reference to the Fermi level of polycrystalline Ag film which was separately determined by LEIPS.

KP measurements were conducted using UHV-KP (KP Technology, UK) installed in the same vacuum system.

Acknowledgements

We thank Dr. Eisuke Ito and Mr. Takumi Aihara for help in data acquisition. This work was supported by JSPS KAKENHI (Grant Number 19K22160) and the Research Grant Program of the Futaba Foundation.

References

[1] J. Pendry, New probe for unoccupied bands at surfaces, Phys. Rev. Lett., 45 (1980) 1356.

[2] G. Denninger, V. Dose, H. Scheidt, A VUV isochromat spectrometer for surface analysis, App. Phys., 18 (1979) 375-380.

[3] D. Funnemann, H. Merz, 10 eV photon detector for inverse photoemission, J. Phys. E: Sci. Instrum., 19 (1986) 554.

[4] M. Budke, V. Renken, H. Liebl, G. Rangelov, M. Donath, Inverse photoemission with energy resolution better than 200 meV, Rev. Sci. Instrum., 78 (2007) 083903.

[5] K. Tsutsumi, H. Yoshida, N. Sato, Unoccupied electronic states in a hexatriacontane thin film studied by inverse photoemission spectroscopy, Chem. Phys. Lett., 361 (2002) 367-373.

[6] P.I. Djurovich, E.I. Mayo, S.R. Forrest, M.E. Thompson, Measurement of the lowest unoccupied molecular orbital energies of molecular organic semiconductors, Org. Electron., 10 (2009) 515-520.

[7] J. Sworakowski, J. Lipiński, K. Janus, On the reliability of determination of energies of HOMO and LUMO levels in organic semiconductors from electrochemical measurements. A simple picture based on the electrostatic model, Org. Electron., 33 (2016) 300-310.

[8] H. Yoshida, Near-ultraviolet inverse photoemission spectroscopy using ultra-low energy electrons, Chem. Phys. Lett., 539-540 (2012) 180-185.

[9] H. Yoshida, Principle and application of low energy inverse photoemission spectroscopy: a new method for measuring unoccupied states of organic semiconductors, J. Electron. Spectrosc. Relat. Phenom., 204 (2015) 116-124.

[10] Y. Zhong, S. Izawa, K. Hashimoto, K. Tajima, T. Koganezawa, H. Yoshida, Crystallization-induced energy level change of [6, 6]-phenyl-c61-butyric acid methyl ester (PCBM) film: Impact of electronic polarization energy, J. Phys. Chem. C, 119 (2015) 23-28.

[11] T. Aihara, S.A. Abd-Rahman, H. Yoshida, Metal screening effect on energy levels at metal/organic interface: Precise determination of screening energy using photoelectron and inverse-photoelectron spectroscopies, Phys. Rev. B, 104 (2021) 085305.

[12] Y. Uemura, S.A. Abd-Rahman, S. Yanagisawa, H. Yoshida, Quantitative analysis of the electrostatic and electronic polarization energies in molecularly mixed films of organic semiconductors, Phys. Rev. B, 102 (2020) 125302.

[13] A. Sugie, W. Han, N. Shioya, T. Hasegawa, H. Yoshida, Structure-dependent electron affinities of perylene diimide-based acceptors, J. Phys. Chem. C, 124 (2020) 9765-9773.

[14] K. Yamada, S. Yanagisawa, T. Koganezawa, K. Mase, N. Sato, H. Yoshida, Impact of the molecular quadrupole moment on ionization energy and electron affinity of organic thin films: experimental determination of electrostatic potential and electronic polarization energies, Phys. Rev. B, 97 (2018) 245206.

[15] H. Yoshida, K. Yamada, J.y. Tsutsumi, N. Sato, Complete description of ionization energy and electron affinity in organic solids: Determining contributions from electronic polarization, energy band dispersion, and molecular orientation, Phys. Rev. B, 92 (2015) 075145.

[16] J. Yang, H. Sato, H. Orio, X. Liu, M. Fahlman, N. Ueno, H. Yoshida, T. Yamada, S. Kera, Accessing the conduction band dispersion in CH3NH3PbI3 single crystals, J. Phys. Chem. Lett., 12 (2021) 3773-3778.

[17] B.W. D'Andrade, S. Datta, S.R. Forrest, P. Djurovich, E. Polikarpov, M.E. Thompson, Relationship between the ionization and oxidation potentials of molecular organic semiconductors, Org. Electron., 6 (2005) 11-20.

[18] J. Sworakowski, K. Janus, On the reliability of determination of energies of HOMO levels in organic semiconducting polymers from electrochemical measurements, Org. Electron., 48 (2017) 46-52.

[19] O.L. Griffith, J.E. Anthony, A.G. Jones, D.L. Lichtenberger, Electronic properties of pentacene versus triisopropylsilylethynyl-substituted pentacene: Environment-dependent effects of the silyl substituent, J. Am. Chem. Soc., 132 (2010) 580-586.

[20] A. Cabrera-Espinoza, B. Insuasty, A. Ortiz, Novel BODIPY-C60 derivatives with tuned photophysical and electron-acceptor properties: Isoxazolino [60] fullerene and pyrrolidino [60] fullerene, J. Lumin., 194 (2018) 729-738.

[21] S.A. Lerke, B. Parkinson, D.H. Evans, P.J. Fagan, Electrochemical studies on metal derivatives of buckminsterfullerene (C60), J. Am. Chem. Soc., 114 (1992) 7807-7813.

[22] Q. Xie, E. Perez-Cordero, L. Echegoyen, Electrochemical detection of C606-and C706-: Enhanced stability of fullerides in solution, J. Am. Chem. Soc., 114 (1992) 3978-3980.

[23] B.W. Larson, J.B. Whitaker, X.-B. Wang, A.A. Popov, G. Rumbles, N. Kopidakis, S.H. Strauss, O.V. Boltalina, Electron affinity of phenyl–C61–butyric acid methyl ester (PCBM), J. Phys. Chem. C, 117 (2013) 14958-14964.

[24] J.D. Anderson, E.M. McDonald, P.A. Lee, Electrochemistry and Electrogenerated Chemiluminescence Processes of the Components of Aluminum Quinolate/Triarylamine, and Related Organic Light-Emitting Diodes, J. Am. Chem. Soc., 120 (1998) 9646-9655.

[25] H. Yoshida, K. Yoshizaki, Electron affinities of organic materials used for organic light-emitting diodes: A low-energy inverse photoemission study, Org. Electron., 20 (2015) 24-30.

[26] W. Han, H. Yoshida, N. Ueno, S. Kera, Electron affinity of pentacene thin film studied by radiation-damage free inverse photoemission spectroscopy, Appl. Phys. Lett., 103 (2013) 123303.

[27] H. Yoshida, Low-energy inverse photoemission study on the electron affinities of fullerene derivatives for organic photovoltaic cells, J. Phys. Chem. C, 118 (2014) 24377-24382.

[28] K. Yamada, R. Shiraishi, K. Nakao, R. Murdey, N. Sato, R. Makino, Y. Suda, K. Yonezawa, T. Yamaguchi, S. Kera, H. Yoshida, A method to evaluate accurate values of the ionization energy

and electron affinity of an organic semiconductor from the electrochemical oxidation and reduction potentials of its component molecule: correction for the electrostatic energy (in preparation).

[29] H. Ishii, K. Sugiyama, E. Ito, K. Seki, Energy level alignment and interfacial electronic structures at organic/metal and organic/organic interfaces, Adv. Mater., 11 (1999) 605-625.

[30] N. Hayashi, H. Ishii, Y. Ouchi, K. Seki, Examination of band bending at buckminsterfullerene (C 60)/metal interfaces by the Kelvin probe method, J. Appl. Phys., 92 (2002) 3784-3793.

[31] S.A. Abd-Rahman, T. Yamaguchi, S. Kera, Y. Hiroyuki, Sample-shape dependent energy levels in organic semiconductors (submitted).

[32] L. Reimer, Transmission Electron Microscopy : Physics of Image Formation and Microanalysis, in: P.W. Hawkes (Ed.), Springer Series in Optical Sciences, vol. 36, Springer, Berlin, Heidelberg, 1997, pp. 463-494.

[33] H. Yoshida, Note: Low energy inverse photoemission spectroscopy apparatus, Rev. Sci. Instrum., 85 (2014) 016101.

[34] F. Amy, C. Chan, A. Kahn, Polarization at the gold/pentacene interface, Org. Electron., 6 (2005) 85-91.

[35] K. Akaike, K. Kanai, H. Yoshida, J.y. Tsutsumi, T. Nishi, N. Sato, Y. Ouchi, K. Seki, Ultraviolet photoelectron spectroscopy and inverse photoemission spectroscopy of [6, 6]-phenyl-C 61-butyric acid methyl ester in gas and solid phases, J. Appl. Phys., 104 (2008) 023710.

[36] Z.-L. Guan, J.B. Kim, H. Wang, C. Jaye, D.A. Fischer, Y.-L. Loo, A. Kahn, Direct determination of the electronic structure of the poly (3-hexylthiophene): phenyl-[6, 6]-C61 butyric acid methyl ester blend, Org. Electron., 11 (2010) 1779-1785.

[37] R. Nakanishi, A. Nogimura, R. Eguchi, K. Kanai, Electronic structure of fullerene derivatives in organic photovoltaics, Org. Electron., 15 (2014) 2912-2921.

[38] K. Akaike, K. Kanai, Y. Ouchi, K. Seki, Side chain effect on electronic structure of spin-coated films of [6, 6]-phenyl-C61-butyric acid methyl ester and its bis-adduct, Chem. Phys., 415 (2013) 31-35.

[39] D.R. Zahn, G.N. Gavrila, M. Gorgoi, The transport gap of organic semiconductors studied using the combination of direct and inverse photoemission, Chem. Phys., 325 (2006) 99-112.

[40] R. Murdey, N. Sato, M. Bouvet, Frontier electronic structures in fluorinated copper phthalocyanine thin films studied using ultraviolet and inverse photoemission spectroscopies, Mol. Cryst. Liq. Cryst., 455 (2006) 211-218.

[41] W. Gao, A. Kahn, Controlled p-doping of zinc phthalocyanine by coevaporation with tetrafluorotetracyanoquinodimethane: A direct and inverse photoemission study, Appl. Phys. Lett., 79 (2001) 4040-4042.

[42] I. Hill, A. Kahn, J. Cornil, D. Dos Santos, J.-L. Brédas, Occupied and unoccupied electronic levels

in organic π-conjugated molecules: comparison between experiment and theory, Chem. Phys. Lett., 317 (2000) 444-450.

[43] I. Hill, A. Kahn, Z. Soos, R. Pascal Jr, Charge-separation energy in films of π-conjugated organic molecules, Chem. Phys. Lett., 327 (2000) 181-188.

[44] Y. Wang, W. Gao, S. Braun, W.R. Salaneck, F. Amy, C. Chan, A. Kahn, Enhancement of iridium-based organic light-emitting diodes by spatial doping of the hole transport layer, Appl. Phys. Lett., 87 (2005) 193501.

[45] W. Gao, A. Kahn, Effect of electrical doping on molecular level alignment at organic–organic heterojunctions, Appl. Phys. Lett., 82 (2003) 4815-4817.

[46] J. Lee, S. Park, Y. Lee, H. Kim, D. Shin, J. Jeong, K. Jeong, S.W. Cho, H. Lee, Y. Yi, Electron transport mechanism of bathocuproine exciton blocking layer in organic photovoltaics, Phys. Chem. Chem. Phys., 18 (2016) 5444-5452.

Supplementary Material

Electron affinities of small-molecule organic semiconductors: Comparison among cyclic voltammetry, conventional inverse photoelectron spectroscopy, and low-energy inverse photoelectron spectroscopy

Mihiro Kubo[a], Hiroyuki Yoshida[b, c, *]

[a]Graduate School of Science and Engineering, Chiba University, 1-33 Yayoi-cho, Inage-ku, Chiba 263-8522, Japan

[b]Graduate School of Engineering, Chiba University, 1-33 Yayoi-cho, Inage-ku, Chiba 263-8522, Japan

[c]Molecular Chirality Research Center, Chiba University, 1-33 Yayoi-cho, Inage-ku, Chiba 263-8522, Japan

*Corresponding author

E-mail address: hyoshida@chiba-u.jp (H. Yoshida)

Table of Contents

1. Solid-state electron affinities and reduction potentials used in this study

Table S1 shows the solid-state electron affinity (A) measured by conventional inverse photoelectron spectroscopy (IPES) and low-energy inverse photoelectron spectroscopy (LEIPS) together with the reduction potential (E_{red}) measured by cyclic voltammetry (CV). The molecular structures appear in Fig. S1. In CV, the first oxidation potential of the ferrocenium/ferrocene (Fc^+/Fc) system is used as a reference. When several values for a molecule are reported, the average value is shown. For pentacene, phthalocyanine, and 6T, A depends on the molecular orientation, that is, standing or lying.

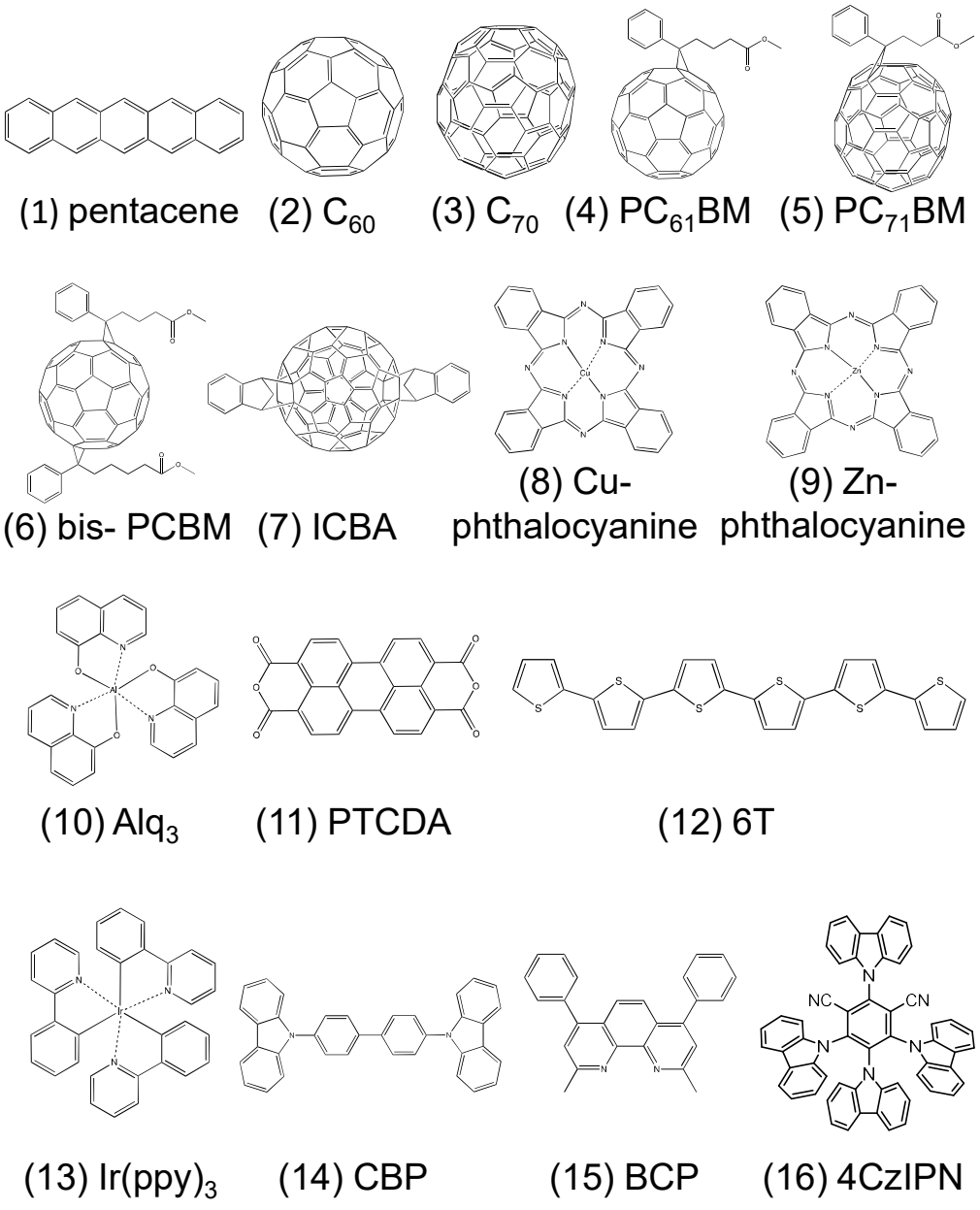

Fig. S1 Molecular structures

Table S1 Solid-state electron affinities A and reduction potentials E_{red} vs Fc^+/Fc.

No.	Compound	A (LEIPS) (eV)	Ref.	A (IPES) (eV)	Ref.	E_{red} (V)	Ref.	E_{red} (V) evaluated
1	Pentacene	2.35 ± 0.02 (standing) 2.7 ± 0.03 (disordered) 3.14 ± 0.02 (lying)	[15] [26]	2.9	[34]	-1.8	[19]	-1.8
2	C_{60}	3.98 ± 0.06	[27]	4.5±0.1 3.98	[35] [36]	-1.00 -0.86 -0.98	[20] [21] [22]	-0.95
3	C_{70}	4.00 ± 0.04	[27]	4.1 ± 0.1	[37]	-0.97	[22]	-0.97
4	$PC_{61}BM$[(a)]	3.76 ± 0.02 (amorphous) 3.64 ± 0.02 (crystalline)	[10]	3.8 3.6 ± 0.1 3.7 ± 0.1	[36] [37] [38]	-1.15	[23]	-1.15
5	$PC_{71}BM$[(b)]	3.81 ± 0.06	[27]	3.7 ± 0.1	[37]			
6	bis-PCBM[(c)]	3.59 ± 0.04	[27]	3.4 ± 0.1 3.2 ± 0.1	[38] [37]			
7	ICBA[(d)]	3.48 ± 0.03	[27]	3.1 ± 0.1	[37]			
8	CuPc[(e)]	3.09 ± 0.05	[8]	2.65 ± 0.2 3.16	[39] [40]			
9	ZnPc[(f)]	3.26 (lying)	[12]	3.34	[41]			
10	Alq_3[(g)]	2.06 ± 0.03	[25]	1.96	[42]	-2.3	[24]	-2.3
11	PTCDA[(h)]	4.11 ± 0.01	[9]	4.6 4.1 ± 0.2	[42] [39]			
12	6T[(i)]	2.17 (standing) 2.75 (lying)	[28]	2.57	[43]*			
13	$Ir(ppy)_3$ [(j)]	1.86 ± 0.05	[25]			-2.71	[25]	-2.71
14	CBP [(k)]	1.75 ± 0.05	[25]	1.92	[44]	-2.75	[6]	-2.75
15	BCP [(l)]	1.89 ± 0.04	[25]	1.70 1.63	[45] [46]	-2.53	[6]	-2.53
16	4CzIPN [(m)]	2.81 ± 0.05	[25]			-1.68	[25]	-1.68
17	IK1 [(o)]	2.22	[25]			-2.29	[25]	
18	IK2 [(o)]	2.10	[25]			-2.36	[25]	
19	IK3 [(o)]	2.35	[25]			-2.20	[25]	
20	IK4 [(o)]	2.36	[25]			-2.01	[25]	
21	IK5 [(o)]	2.10	[25]			-2.40	[25]	
22	IK6 [(o)]	2.62	[25]			-2.11	[25]	
23	IK7 [(o)]	2.30	[25]			-2.33	[25]	
24	IK8 [(o)]	2.46	[25]			-2.27	[25]	
25	IK9 [(o)]	2.35	[25]			-2.09	[25]	
26	IK10 [(o)]	2.35	[25]			-2.09	[25]	
27	IK11 [(o)]	2.45	[25]			-2.05	[25]	
28	IK12 [(o)]	2.39	[25]			-2.14	[25]	
29	IK13 [(o)]	1.66	[25]			-2.72	[25]	
30	IK14[(o)]	1.71	[25]			-2.77	[25]	

(a) (6,6)-phenyl C61 butyric acid methyl ester, (b) (6,6)-phenyl C71 butyric acid methyl ester, (c) bis(1-[3-(methoxycarbonyl)propyl]-1-phenyl)-[6,6]C62, (d) indene-C60 bisadduct, or 1',1'',4',4''-tetrahydro-di[1,4]methanonaphthaleno[5,6]fullerene-C60, (e) Copper(II) phthalocyanine, (f) Zinc(II) phthalocyanine, (g) tris(8-hydroxyquinoline)aluminum(III), (h) 3,4,9,10-perylene tetracalboxylic dianhydride, (i) alpha-sexithiophene, (j) tris(2-phenylpyridine)iridium(III), (k) 4,4′-Bis(N-carbazolyl)-1,1′-biphenyl, (l) bathocuproine, (m) 2,4,5,6-Tetra(9H-carbazol-9-yl) isophthalonitrile, (o) compound by Idemitsu Kosan Co., Ltd., whose molecular structure is undisclosed.

*The workfunction is not given in Ref. [43].

2. Correlation between reduction potentials (E_{red}) used in this study and a previous study

Figure S2 shows the correlation between E_{red} values used in this study and a previous study [7]. The values of E_{red} are taken from the references listed in Table S1. We found a good linear correlation, which is expressed as

$$E_{red}\,(\text{this study}) = (1.02 \pm 0.03) \times E_{red}\,(\text{previous study}) + (0.01 \pm 0.05). \qquad \text{(S1)}$$

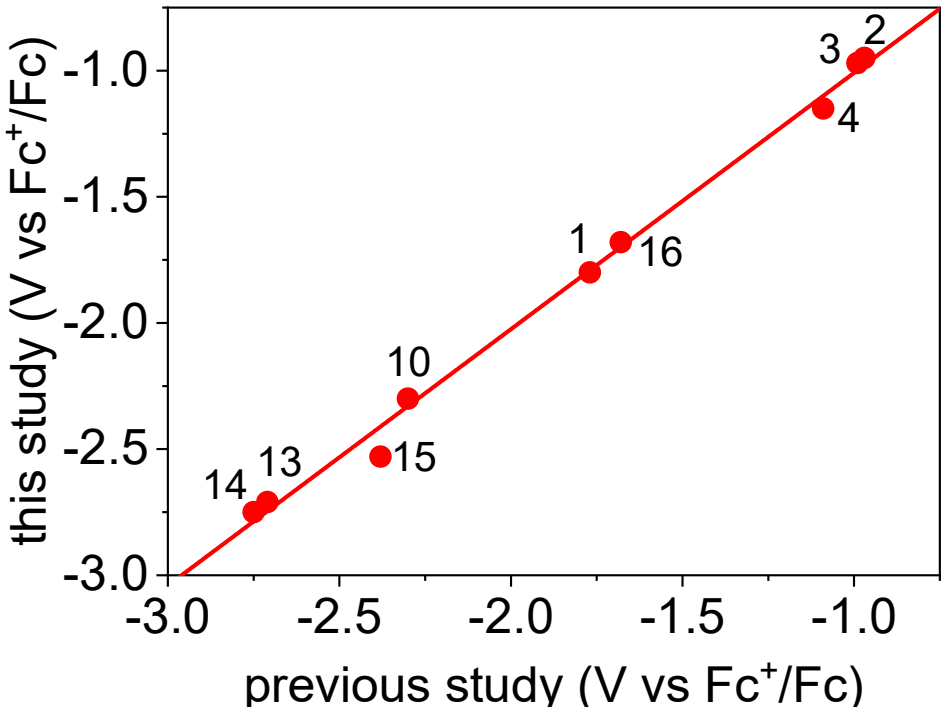

Fig. S2 Correlation between reduction potentials (E_{red}) used in this study and a previous study [7]. Data are evaluated for the nine compounds listed in Table S1. The red line is the linear correlation expressed as Eq. S1.